Contributions to Geophysics and Geodesy Vol. 55/1, 2025 (85–113)

The use of space geophysics data to establish a subsurface structural frameworks map on East Uweinat ring complexes province, Southwestern Desert, Egypt

Yaseen AAMER[1,*], Ashraf GHONEIMI[2], Salah HANAFY[1], Mohamed H. M. YOUSEF[1], Sara ZAMZAM[2]

[1] Nuclear Materials Authority, P.O. Box 530, Maadi, Cairo, Egypt

[2] Department of Geology, Faculty of Science, Zagazig University, P.O. Box, 44519 Zagazig, Egypt

Abstract: The study focuses on the east Uweinat area in the eastern sector of the Saharan continental crust and extends to the Arabian-Nubian basement rocks in the east. This area extends beyond the Egyptian territories, including the northern part of Sudan and the eastern part of Libya. The Saharan continental crust represents a challenge due to its classification as an arid to hyper arid environment and the difficulty of accessing it. The study aims to construct the regional structural framework of the basement complex that has its influence on the overlying sedimentary section, specifically in the part that belongs to the Saharan continental crust of Egypt. Space geophysical data was used, including GRACE, magnetic, SRTM Gravity Recovery and Climate Experiment, Earth Magnetic Anomaly Grid, Shuttle Radar Topographic Mission and geoid data. A qualitative and quantitative interpretation is used to highlight the subsurface geological picture and structure framework. The integration of these data helps to understand the subsurface structural framework and provide insights into the geological evolution of the region. The constructed structural framework map shows the presence of a large basin east of the Uweinat area, mainly sourced from the Nile River and a small amount of rainfall, with geological obstacles preventing water leakage out. The occurrence of the East Uweinat ring complexes and volcanism have both positive and negative impacts and must be taken into account in any systematic natural resources exploration strategy.

Key words: EMAG2, SRTM, GRACE, geoid, structural modelling

1. Introduction

Africa is one of the continents that were subjected to many orogenic episodes or tectonic events over the course of geological time, from the beginning of

*corresponding author, e-mail: yaseen.aamer.1234@gmail.com

doi: 10.31577/congeo.2025.55.1.6

the cratons formation at Paleoarchean to Mesozoic-Cenozoic Eras. It preserves approximately 75% of Earth's history (*Choubert and Faure-Muret, 1990; Gubanov and Mooney, 2009; Van Hinsbergen et al., 2011*).

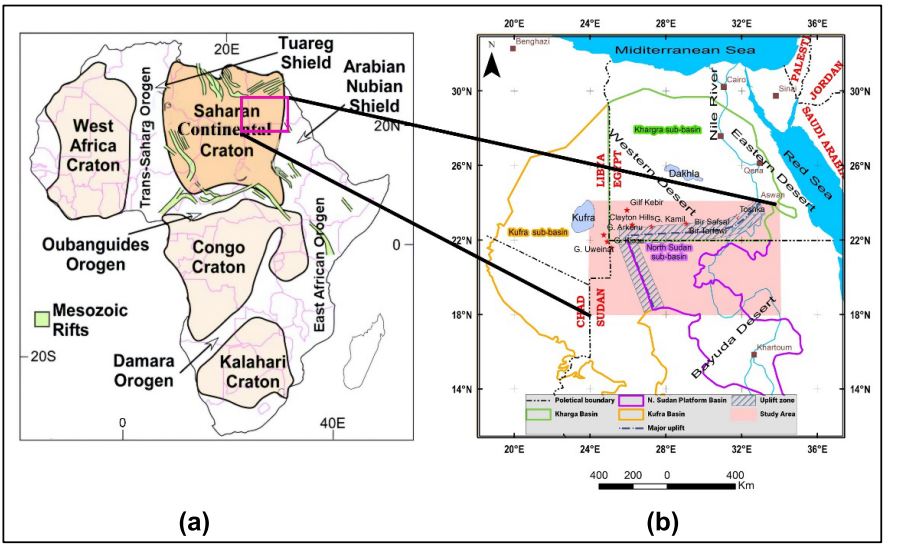

Fig. 1. (a) Saharan Metacraton of Africa (modified after *Abdelsalam et al., 2011*); (b) location of the study area (modified after *Mohamed et al., 2022*) in relation to (a).

Africa consists mainly of four Archean cratons, which are surrounded by belts that were metamorphosed or deformed throughout the Pan-African orogeny at Early Paleozoic (*Giresse, 2008*) (Fig. 1a). The Saharan continental crust/craton (SCC) is one of these cratons. It hosts three proposed ancient areas, which are probably marked at the surface by metamorphosed remnant Paleoproterozoic and Archean terranes with thicker lithosphere that extends to 200 km including: Al Kufrah (A) in the Northeast, Murzuk (B) in the Northwest, and Chad (C) at the south (*Fezaa et al., 2010; Liégeois et al., 2013*). The SCC occupies about 5 million km^2 at the north to central region of Africa, which extends relatively to ten countries and is bordered on the east by the Arabian-Nubian Shield (ANS) and on the west by the Tuareg Shield (*Abdelsalam et al., 2002*). It is surrounded to the north by Phanerozoic rocks of the African continent and to the south by the Congo Craton (Fig. 1a). The SCC is characterized by its ambiguity due to the poorly isolated Precambrian terranes (medium to high-grade rocks) that

exposed within extensive Phanerozoic (Cretaceous and younger) cover. The oldest basement rocks in the SCC are located at the inside of Gabel (G.) Uweinat as well as (G.) Kamil, that is relatively near the centre of the SCC (Fig. 1b). The SCC is the focus of attention of many researchers, especially groundwater explorers, due to the presence of the Nubian sandstone, which is considered one of the major aquifer system in Africa. Therefore, there is controversy so far among many studies about the nature of the composition of its rocks, and so the extent to which they are affected by different tectonic events. These researches focused on the limited exposed Precambrian rocks of the eastern, western, and southern boundaries (*Abdelsalam et al., 2011; Bea et al., 2011b; Blades et al., 2021; Fezaa et al., 2010; Karmakar and Schenk, 2015*).

Although various geophysical investigations have been applied on Africa cratons as a whole or parts of them, there are few in comparison to other studies, especially at the eastern part of the SCC. Seismic tomography, gravity, geoid, heat flow and electrical resistivity data were the most utilized methods for studying its rheological characteristics, giving an imaging of its evolution, and structural framework, such as (*Haas et al., 2021; Jessell et al., 2016; Le Pape et al., 2021; Lebedev et al., 2009; Olugboji et al., 2024; Senosy et al., 2013; Sobh et al., 2020*). Moreover, other researches that were concerned with studying the hydrogeological features in general, in order to delineate groundwater aquifers, particularly southern part of Egypt (*Ibrahim et al., 2023*). Geophysical techniques were applied either alone or in combination to achieve the objectives of these studies. *Senosy et al. (2013)* used geophysical methods, particularly the gravity method, to study the subsurface geology and detect subsurface structures and tectonic framework of east Uweinat area.

The current research includes studying the eastern sector of the SCC and extends to the (ANS) basement rocks at the east. It covers the region between latitude 18°00′ to 25°00′ N and longitude 24°00′ to 34°00′ E (Fig. 1). The region extended outside the Egyptian territories to include the northern part of Sudan and the eastern part of Libya. The studied area is classified as arid to hyper arid environment, as it characterized by general scarcity of rainfall rates throughout the year, except short, intermittent, and scattered seasonal rates (*Sudan Environment Report, 2020*). The area is occupied by complex structures developed due to the interaction of various tectonic

events, including those that shaped the SCC. The SCC formed during the Archean-Paleoproterozoic and was later reactivated by Neoproterozoic tectonics (*Abdelsalam et al., 2002*). The Bayudian Event (∼ 920–900 Ma) initiated magmatism in Sudan's Bayuda Desert (*Küster et al., 2008*), followed by pre-Pan-African deformation (∼ 860–750 Ma), which was characterized by localized collisions and granitoid intrusions (*Abdelsalam et al., 2011*). The main Pan-African orogeny (˜650–580 Ma) led to a collision with the (ANS), causing metamorphism and post-collisional magmatism, with effects extending into Chad (*Fritz et al., 2013; Shellnutt et al., 2018*). By ∼ 580 Ma, lithospheric delamination triggered A-type granite formation (*Shellnutt et al., 2019*), and final stabilization by ∼ 500–450 Ma resulted in erosion and sediment deposition across the Saharan Platform (*Liégeois et al., 2013*). These tectonic events collectively contributed to the formation of the complex structural framework in the area. Since the study area is located in the Western Desert of EGYPT, several authors constructed structural maps in order to identify the subsurface basement structure. *Schandelmeier et al. (1983)* mapped the distribution of basement rocks in the Uweinat area using various methods, including geological interpretation maps, satellite images, and gravity and airborne magnetic maps. The structural framework of the Uweinat area includes a general foliation trend of NE–SW, with dips mainly to the northwest and subordinate dips to the southeast.

Consequently, the main objective of this study is to decipher the ambiguity and semantics of the investigated area, which has few exposed rock units cover to map the basement rock distribution as generated from the utilized geospatial data. Furthermore, we present a detailed surface, subsurface structural model and their relative sedimentary basins depths for giving clear and comprehensive results to be used in future studies that concerned with assessment of the groundwater potentiality in a global perspective for the developing and economical activities. These goals will be achieved using multiple space-based spatial data such as Gravity Recovery and Climate Experiment (GRACE), Earth Magnetic Anomaly Grid (EMAG2), Shuttle Radar Topographic Mission (SRTM) DEM, as well as supplementary geological units, and surface structural features. The utilized data have their own behaviour to reach the best possible results of the investigated area in an integrated manner. In addition, they assist to overcome the ambiguous in the interpretation of each of them.

2. Regional geological and tectonic settings

The study area is characterized by the presence of various lithological units that represent most of the geological Eras and tectonic events as shown in (Fig. 2). Precambrian rocks in the current area show diverse textural and compositional criteria, which range in their age between 2656 to 650 Ma (*Stern, 2018; Zimmer et al., 1995*). In general, these rock units are gradually getting younger eastward where along the Red Sea coast, the (ANS) (Fig. 1a) as well as to the south direction (*Stern, 2018*).

Gabel Uweinat and Kamil basement complex at the triple junction area along Egypt, Sudan, and Libya, in the western part of the study area are the oldest rocks with Archean ages. Based on the decratonization during the Neoproterozoic as a result of Pan-African event, the rocks at Uweinat and Kamil revealed two stages of metamorphic evolution.

In general, series of high grade metamorphic formations are exposed on the eastern, southern slopes of (G.) Uweinat and nearby (G.) Kamil region such as migmatitic gneisses and migmatites as well as partly granulites with intercalated marbles, amphibolites and calcsilicates rocks (*Harris et al., 1984; Richter, 1986*). As for Precambrian rocks belonging to ANS at the eastern and southern parts, it consists of extensive volcano-sedimentary-ophiolitic and granitoid assemblage (*Bernau et al., 1987*).

El-Gaby et al. (1988) believed that the Archean-early Proterozoic continental crust enlarged eastward underneath the Pan-African rock units. Tectonically, the old continental crust with unclear deformational history was horizontally accreted and collided with some intra-oceanic ones during the Neo-Proterozoic era forming the (ANS) at the east. This convergent event accompanied by magmatic activity (*Kennedy, 1964*). The regional structural features that affect Precambrian rocks represented by NW–SE to WNW–ESE, N–S, E–W and remnant of older N- to NE- trending thrust faults (*Abdelsalam et al., 2011*).

Due to the ancient age of the study region and the complex tectonic events it was exposed to, whose origin and beginning of occurrence were previously mentioned, Phanerozoic rocks are distinguished by their diversity in terms of their formation time, type, thickness and the surface geological structures affecting them. In contrast to the spatial distribution of Precambrian rocks, Phanerozoic rocks cover large areas in the investigated region (Fig. 2). Phanerozoic sediments filling up low topography, however,

the basement rocks and sediments were both invaded by volcanics created local sub-basins in the basement.

The Paleozoic exposures are restricted at localized areas in the northwest of the Gilf Kebir and Uweinat area in Egypt and Libya as well as in the far southwest corner of the study area in Sudan (Fig. 2). These rocks may be of Cambro-Ordovician-Silurian age and consist of thick coarse grained sandstone, relatively 200 m except at southeast of (G.) Kissu (*Jux and Issawi, 1983*).

Contrary, Paleozoic and Mesozoic strata are the largest ones that extend over large areas (Fig. 2). These units are represented by sandstone layers (dip northwards) of Devonian and Cretaceous ages that named the Nubian Sandstone Formation. This Formation is classified into three distinctive sub-basins based on their location and thicknesses (*Mohamed et al., 2017; Thorweihe, 1986*). The Kufra sub-basin is the largest one that expands across Libya, northwestern Sudan and northeastern Chad (approximately 4000 m), while the Northern Sudan Platform sub-basin is the smallest one (relatively 500 m). The third is the Dakhla sub-basin which exposed in Egypt with 3000 m thickness (Fig. 1a, *Klitzsch and Lejal-Nicol, 1984; Mohamed et al., 2017*).

To the east of Gabel Uweinat, the surface of the East Uweinat area is underlain by Mesozoic sediments attributed, in most of the area, to the lowermost part of the Nubia Sandstone sequences, which dip northwards. However, these sediments are extensively covered by dunes. Some minor intrusions were emplaced into the basement and occasionally the cover sedimentary rocks (*Nour, 1996*). To the west, the Gilf Kebir (the Great Barrier) is a great plateau of Paleozoic sandstones sequence lies as that of G. Uweinat directly on outcropping Precambrian basement.

According to *Hesse et al. (1987)*, Tertiary sediments that exposed in the study area are represented by silt and clay intercalations of deltaic origin. On the other hand, the basement and occasionally Paleozoic and Mesozoic sedimentary rocks have been intruded by distinctive plugs of volcanic intrusions of alkaline and basic composition dykes and granite complexes of Tertiary age (*Bea et al., 2011a*). These volcanic activities are the three ring complexes of the Uweinat province widely distributed in G. Uweinat, G. Arkenu and G. Kissu. Geologically the G. Uweinat is composed of two very different parts. The western part, lying entirely in Libya, is composed

on a large granite ring complex, about 25 km in diameter. The southern half is less eroded; there a large crescent shaped plateau fills the interior of the ring, much dissected by shallow water courses. The eastern part consists of a large block of Paleozoic sandstone, resting upon metamorphosed Precambrian basement rocks, propped against the granite uplift to the west. G. Arkenu is lying about 25 km to the north-west. It is smaller granite ring complex, with a broken interior drained by one main wadi system. To the northeast there is the much-eroded remnant of a sandstone massif adjacent to the granite dome. Slightly further to the south is the massif of Kissu. This ring complex is very similar to those in Arkenu and Uweinat. The three igneous activities have occurred probably in the Late Eocene age from 45 to 42 ± 1 Ma (*Vail, 1976*). The Clayton hills are ring like craters of apparently volcanic origin, probably of similar age of Uweinat occurrence.

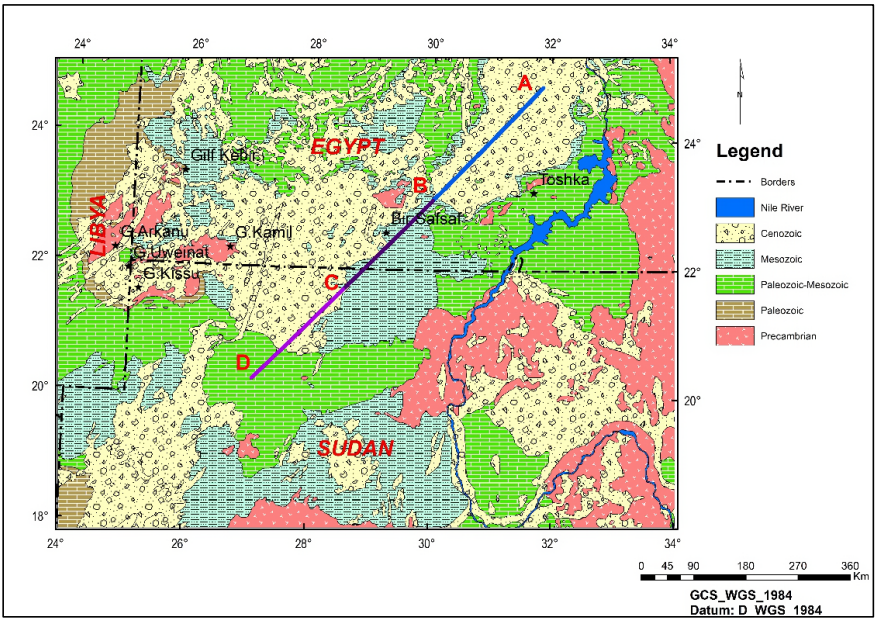

Fig. 2. Generalized geological map of the study area modified after *Persits et al. (1997)*.

Hanafy (2014) traced the track (Pre-I) of the hot spot activity from the Late Precambrian/Cambrian, where the magmatism started 593 ± 16 Ma through three ring complexes (Saint Catherine, Ras Zeit and Wadi Dib) to the granitic ring complexes exposure of Uweinat province and the volcanic

eruptions of Late Eocene (Fig. 3), where magmatism recurrent with high intensity towards the SW of Egypt. This track is an excellent example of the type of composite alkaline igneous ring complexes associated with continental rifts worldwide.

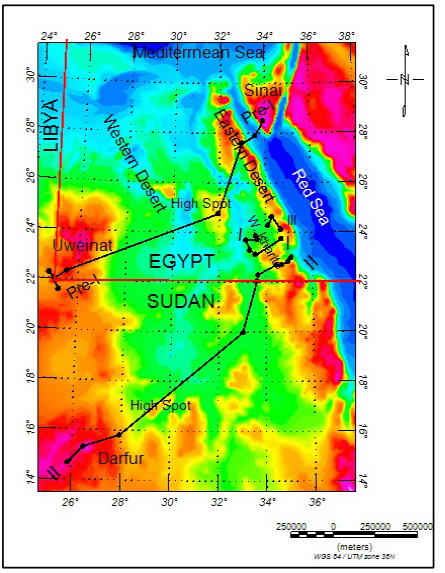

Fig. 3. Tracks of the four phases of the Late and Post Precambrian igneous activity of the study area after (*Hanafy, 2014*).

3. Space geophysics data and methodology

In this study, various geospatial datasets were utilized, including the high-resolution 30 m (1 arc/sec) NASA Shuttle Radar Topography Mission (SRTM) Digital Elevation Model (*U.S. Geological Survey, 2019*), the recently published Gravity Recovery and Climate Experiment (GRACE) Global Geopotential Model (*ICGEM, n.d.*), the Earth Gravitational Model (EGM2008) for geoid departure data (*ICGEM, n.d.*), and the Earth Magnetic Anomaly Grid 2 (EMAG2) dataset (*Maus, 2009*). These datasets were optimally combined to enhance the regional gravity geodetic model, with integration performed at a grid resolution of 2 arc/minute ($\sim$3.7 km). The references provided correspond to the official sources from which these datasets were obtained.

Earth's magnetic anomalies (EMAG2) compiled from satellite, ship and airborne magnetic measurements. These maps increase knowledge of subsurface and crustal structure and the study of lithosphere evolution (*Benahmed Daho et al., 2009*).

The GRACE satellite mission, launched in 2002 by NASA and the German Aerospace Center (DLR), measures variations in Earth's gravity field caused by mass redistribution on and beneath the surface (*Chen et al., 2022*). The study utilizes the GGM02C model (GRACE Gravity Model 02C), which is a static, time-independent gravity field model with a maximum spherical harmonic degree and order of 200 (*Tapley et al., 2005*).

The geoid represents an equipotential surface of the Earth's gravity field, reflecting mass distribution variations within the lithosphere and mantle (*Steinberger, 2016*). The dataset used in this study is based on the EGM2008 global geoid model, which provides high-resolution geoid height variations derived from satellite gravimetry and terrestrial gravity data (*Pavlis et al., 2012*). This model has been widely applied in studies of mantle convection, lithospheric deformation, and hotspot activity (*Lemenkova, 2023; Prasad et al., 2021; Wu et al., 2018*). The fine-scale resolution of EGM2008 (up to degree and order 2190) makes it particularly useful for analyzing regional geoid anomalies and their geological implications (*Corchete, 2010*).

Generally, DEMs hold an essential role for large diversity of applications, including modelling of hydrological processes, geomorphological mapping and various other forms of spatial analyses incorporating three or more dimensions (*Braun, 2021; Maune et al., 2007; Schillaci et al., 2015*). The most spatial resolution it is, the most effective and accurate it is in the results of studies. Thus, in the current study, a high-resolution SRTM DEM (30 m) was utilized primarily for assessment the surface topographical features and surface structural mapping.

Gridding, processing, and depth to basement were calculated using Oasis montage data processing and analysis system (*Geosoft Oasis montaj – Seequent, n.d.*). 2-D simultaneous magnetic modelling was carried out using GM-SYS software program (Building and Managing 2D Models in GM-SYS – *Geosoft Oasis montaj – Seequent, n.d.*). Since both gravity and magnetic methods make use of natural potential fields, the procedures for interpreting magnetic anomalies and gravity anomalies are similar basing its rules of attraction on the inverse square. However, some variations make mag-

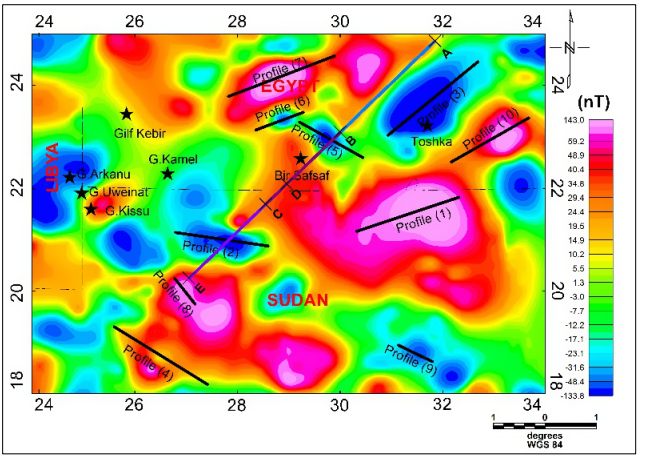

Fig. 4. Magnetic anomaly map of the study area extracted from the EMAG2 grid, (A–B), (B–C), (D–E) lines are model profiles, while profiles 1–10 are used for depth estimation.

netic interpretation more challenging (*Kearey and Brooks, 1991*). Gravity method measure variations in the Earth's gravitational field to infer density contrasts and are typically used to identify large-scale geological structures such as faults and sedimentary basins. The interpretation of gravity data can be non-unique due to the ambiguity of density distributions, requiring supplementary data for precise conclusions (*Hinze et al., 2013*). Magnetic methods measure variations in the Earth's magnetic field, focusing on the distribution of magnetic minerals, and are particularly effective in mapping shallow subsurface features and mineral deposits. Magnetic data interpretation can be complex due to the dipolar nature of magnetic anomalies and the influence of remanent magnetization, yet it allows for high-resolution imaging and depth estimation (*Butler, 2007*).

3.1. Qualitative interpretation

3.1.1. Magnetic

The magnetic map can reveal information on the composition and underlying structure of the Earth's crust (*Saad et al., 2010*). The EMAG2 was used to generate the datasets for magnetic anomalies. Close investigation of the magnetic intensity map (Fig. 4) indicates that it can be divided to several zones according to the magnetic amplitude. The highest magnetic ampli-

tude values concentrate in the central and eastern parts of the study area that has nearly NE and NW trends, meanwhile the low amplitude values are concentrated in the western side. There is also a low amplitude values zone in the northeastern side where the lowest recorded magnetic amplitude value exists. Some lower magnetic amplitude zones are scattered in the southwestern and southeastern sides of the study area. This variation can be attributed to differences in magnetic susceptibility and geological structures since different types of rocks and minerals have varying magnetic susceptibility. Areas with high-susceptibility materials, like iron-rich rocks, will produce stronger magnetic anomalies compared to areas with low-susceptibility materials (*Liu and Hu, 2018*).

3.1.2. SRTM

The study area has a clear difference in elevations between the west and the east, which shows gradual decreasing and has nearly NE–SW trend. The high-elevated areas are concentrated in the western part (560–1057 m), such as G. Uweinat in in the Egyptian/Libyan desert (Fig. 5). The plain between Uweinat and Al-Gelf Al-Kabir is dotted with groups of low hills that remotely resemble other flat masses in the region. While the elevation of the surface decreases sharply toward the centre of the region as indicated by condensed contours, and then decreases gradually in the direction of the east (The Nile Valley). The Nile Valley is a fertile strip that runs

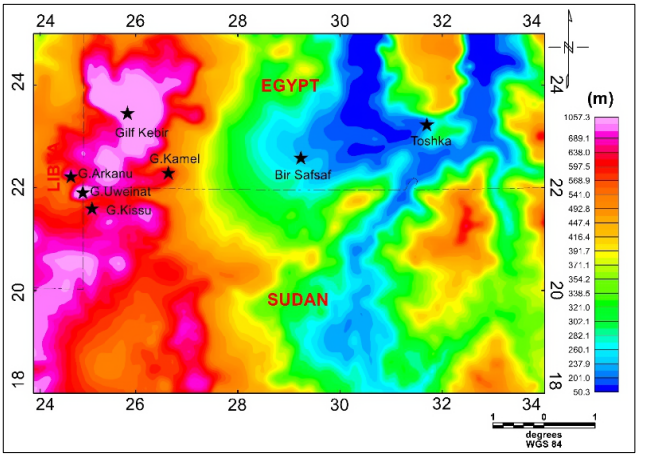

Fig. 5. SRTM Digital Elevation Model map of the study area.

parallel to the river, in contrast to the arid and rocky desert regions on either side of it. The low-elevated topography in the east is interrupted by some uplifted regions, reaching an elevation of about 550 m (Fig. 5). These uplifted regions may be caused by crustal flexure that accompanied the formation of sedimentary basins, particularly at the north part of the study area such as Kharga basin. The ground surface of the east Uweinat area slopes from west to east and from south to north, forming a flat, sandy environment.

3.1.3. Complete Bouguer gravity anomalies

The Gravity Recovery and Climate Experiment (GRACE) mission has significantly improved global gravity field models by providing high-accuracy, long-wavelength gravity data. Although GRACE is primarily designed for monitoring time-variable gravity changes, its derived static models, such as GGM02C, offer superior gravity accuracy compared to pre-GRACE models like EGM96. These static models have been widely applied in geophysical studies, particularly in tectonic and structural mapping.

In this study, we used the GGM02C global gravity model as the basis for generating the Complete Bouguer Gravity Anomalies (CBAs) map (Fig. 6). GGM02C provides a static gravity field representation, making it well-suited for analysing regional tectonic structures rather than transient mass variations (e.g., hydrology or glacial melting). Previous studies, such as (*Mono et al., 2024*), have successfully applied GGM02C for fault detection and depth estimation, demonstrating its effectiveness in structural interpretation. To compute the CBAs, we applied a Bouguer correction, which removes the topographic effect using a 30m resolution Shuttle Radar Topography Mission (SRTM) digital terrain model (DTM). This process converts the free-air gravity anomalies to CBAs, making them more suitable for investigating deep crustal structures.

Complete Bouguer Gravity Anomalies (CBAs) map derived from GRACE satellite Mission (Fig. 6) indicates different gravity signatures that are related to variations in the density of the subsurface materials and geological structures. Igneous complexes of dominant acid composition are characterized by low gravity values and those of dominant basic lithology are indicated by positive gravity signature. The most remarkable gravity anomaly of the area is seen as a large scaled high gravity anomaly with high amplitude

positive responses in the western part of area, which indicates great density contrasts with the surrounding country rock. Whereas the very low value is found in the centre and northeastern part of the study area. These igneous rocks are hereafter referred to as high spot activity widespread intrusive and extrusive bodies within the basins have been mapped. Numerous Craters, dykes, volcanic cones, and lava flows are spectacularly imaged, showing a range of morphologies. According to (*Fairhead and Okereke, 1988*), the existence of the negative anomalies is accompanied to domal uplift structure of the Cenozoic high spot activity and processes related to the East African rift system or generally a result of subsurface low density upper mantle structure (*Sobh et al., 2020*).

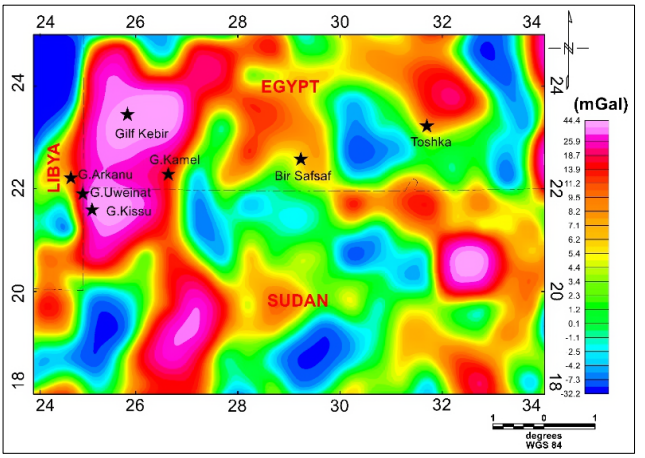

Fig. 6. Complete Bouguer Gravity Anomalies (CBAs) map of the study area.

3.1.4. Geoid model

Geoid relief in the study area is primarily shaped by the heterogeneous structure of the lower mantle and the layered effects of the upper mantle, which collectively influence geoid anomalies. Positive geoid anomalies, such as those observed in the western part of the study area (Fig. 7), are often associated with mantle plumes—buoyant upwellings of hot material from the deep mantle (*Steinberger et al., 2021*). These plumes cause the overlying lithosphere to uplift, contributing to localized geoid heights. The geoid highs observed in the study area, exceeding 12 meters in relief, strongly correlate with elevation variations and regional geological structures.

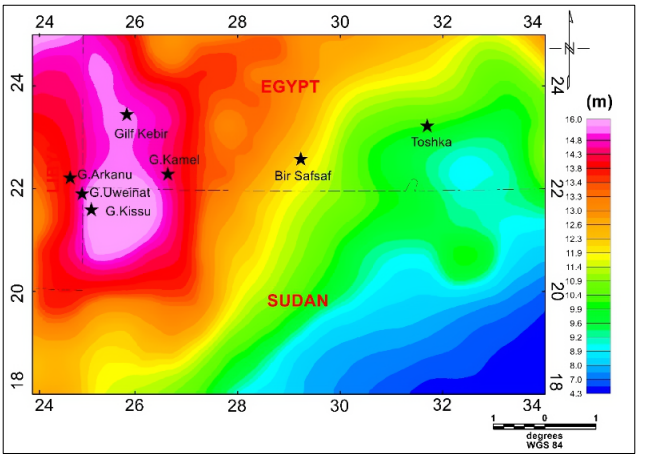

Fig. 7. Departure of the geoid from reference ellipsoid map of the study area.

A striking feature of the geoid map (Fig. 7) is the prominent geoid high in the west and southwestern region, which corresponds to the G. Uweinat, G. Arkenu, and G. Kissu ring complexes. This region exhibits a nearly circular high-relief geoid closure, suggesting a direct link between deep-seated mantle processes and surface topography. The alignment of these geoid anomalies with known hotspot tracks supports the hypothesis that these ring complexes were influenced by Late Eocene mantle plume activity (*Hanafy, 2014; Keppie et al., 2011*). The steep southeastward decrease in geoid relief further highlights the spatial influence of plume-induced uplift and subsequent lithospheric adjustments.

3.2. Quantitative interpretation

3.2.1. Isolation of anomalies

A major step in the analysis of potential field data is the process of isolating the observed anomaly pattern into regional and residual components. This provides the interpreter with valuable information that helps in the delineation of the subsurface geological and structural setting in an area (*Aboelkhair and Rabei, 2013*). The spectral analysis using MAGMAP 2D-FFT system Oasis montaj supports the common Fourier domain filters to the magnetic and gravity gridded data. The band pass filter is excellent

for applying a straightforward high pass and low pass application. The data were transformed to the wave number domain. The azimuthally averaged logarithmic power spectrum was computed. The log spectrum shows two parts, where the spectral slope technique was applied to each. Isolation of the magnetic and gravity anomalies using the band pass filter regional/residual separation filter was conducted.

The interactive spectrum technique was applied to each of them. The residual map (Figs. 8a, 9a) exhibits the local anomalies, which reflect the near-surface structures, while the regional map (Figs. 8b, 9b) reflects the broad anomalies related to the deep-seated changes in the composition of the Basement rocks.

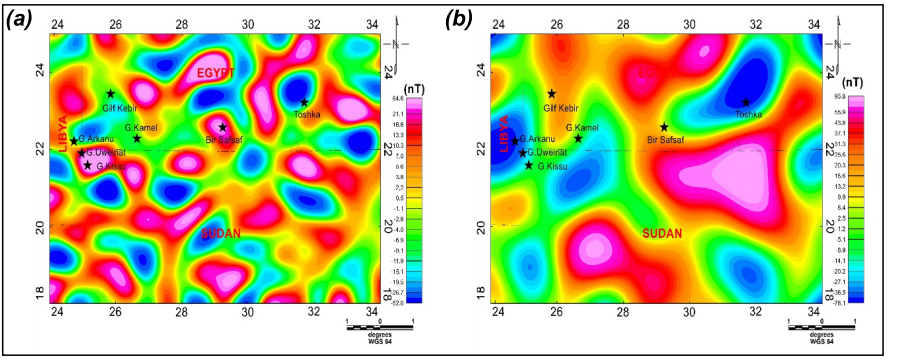

Fig. 8. Colour map of the residual magnetic component (a); the regional magnetic component (b) of the study area.

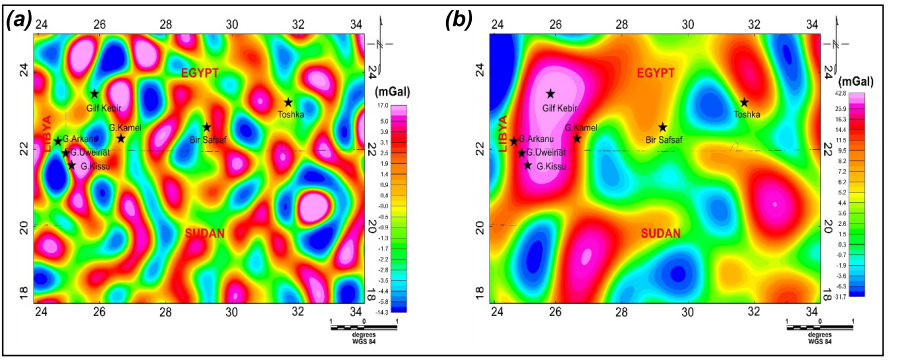

Fig. 9. Colour map of the residual GRACE gravity component (a); the regional GRACE gravity component (b) of the study area.

3.2.2. Trend analysis

Statical trend analysis is an extremely significant strategy in the quantitative interpretation of potential field data. This trend analysis could reveal the directions of forces and their strengths (*Khalil et al., 2016*). Traditional methods for recognizing structural lineaments from magnetic and gravity data often involve manual interpretation techniques that focus on the detection of anomaly centres to delineate subsurface geological structures. These techniques typically rely on identifying and enhancing the magnetic anomalies associated with lineaments, which are often indicative of faults, fractures, or other tectonic features (*Sun et al., 2023*). The structural lineaments at shallow and deep situations of the study area were deduced from the magnetic, residual and regional components maps (Figs. 4, 8a and 8b) as well as from GRACE gravity, residual and regional components maps (Figs. 6, 9a and 9b).

Rose diagrams were constructed for the interpreted structural lineaments in order to assist in defining the principal structural trends in the study area. Generally, the southwestern desert of Egypt, including the Uweinat area, is influenced by prominent tectonic trends primarily oriented NE–SW, E–W, N–S, and NW–SE. These trends, revealed through space-based gravity and magnetic datasets, highlight significant fault lines and structural deformations that shape the region's geological and tectonic framework (*Bakheit et al., 2014; Issawi, 1980*).

The rose diagram of the magnetic map (Fig. 10a) shows that the NE–SW, WNW–ESE, NNW–SSE and E–W trends dominate this map and are arranged in decreasing order of magnitude. These trends are associated with near-surface and deep structures in the study area. For the regional magnetic map (Fig. 10b), the affected deep structures have WNW–ESE, ENE–WSW, NE–SW and NNW–SSE trends, meanwhile the residual magnetic map (Fig. 10c), the affected near-surface structures show that WNW–ESE, ENE–WSW, NE–SW and E–W trends.

The rose diagram of the GRACE Gravity map (Fig. 10d) shows that the NNE–SSW, NW–SE, NE–SW and E–W trends dominate this map and are arranged in decreasing order of magnitude. These trends are associated with near-surface and deep structures in the study area. For the regional Gravity map (Fig. 10e), the affected deep structures have the NE–SW, NNW–SSE, ENE–WSW and WNW–ESE trends, meanwhile the residual gravity map

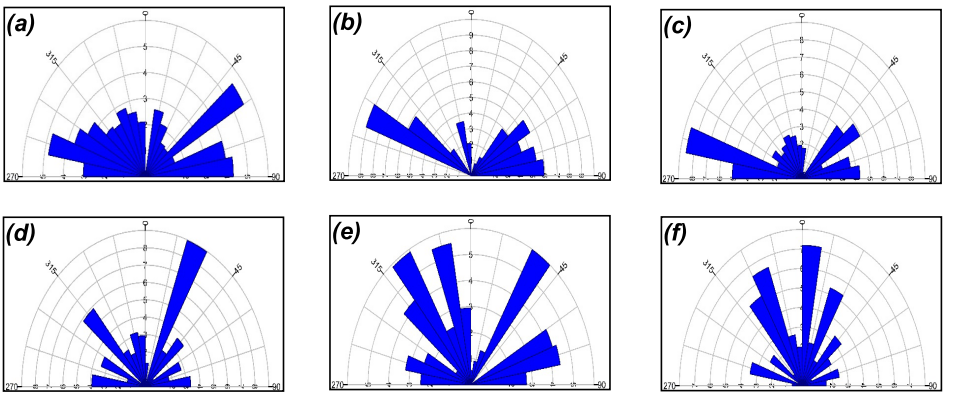

Fig. 10. Rose diagrams showing the main structural lineaments as deduced from (a) magnetic map, (b) regional magnetic map, (c) residual magnetic map, (d) gravity map, (e) regional gravity map, (f) residual gravity map of the study area.

(Fig. 10f), the affected near-surface structures show that nearly N–S with NNW–SSE, NE–SW and WNW–ESE trends.

3.2.3. Depth computation results and 2D magnetic modelling

Depth estimation plays an important role in magnetic interpretations. The depth of ten magnetic anomaly sources distributed across the study area (Fig. 4) was calculated using Peter's manual half-slope method (*Peters, 1949*).

The results for all profiles are summarized in Table 1.

Table 1. Depth estimation results for magnetic anomaly sources using Peter's half-slope method.

Profile No.	Depth (m)	Profile No.	Depth (m)
1	500	6	275
2	130	7	165
3	680	8	150
4	190	9	201
5	470	10	190

The GM-SYS profile is a program for computing magnetic response from a cross-section of geologic models (*Mehanee, 2022*). The application of algorithms described by (*Won and Bevis, 1987*) enabled the forward modelling

procedure to create a hypothetical geologic model and compute the magnetic responses based on (*Talwani et al., 1959*). The magnetic gridded data used for modelling were obtained along three profiles (A–B), (B–C), and (D–E), all trending from NE to SW. Figure 4 illustrates the locations of these profiles, and the following sentences will describe in detail their results.

2D profile (A–B)

The first profile (A–B) is located to the northeast of the study area and displays the variations in the basement surface with a total length of about 272 km (Fig. 11a). Upon inspection of this profile, this profile reveals an agreement between the estimated and observed anomalies with a root mean square error of 1.317 nT. The upper section of this model represents sedimentary rocks with a magnetic susceptibility of 0 in c.g.s units. The lower section represents the basement rocks, consisting of three blocks: the first is found in the northeastern part of the profile, the second is nearly in the middle, and the third is found in the southwestern part of the profile. The magnetic susceptibilities of these blocks are 0.00965, 0.00975, and 0.0092 in c.g.s. units, respectively. The basement surface slopes downward from the northeast to the southwest, with varying depths that vary from 50 to 1000 metres below the surface.

2D profile (B–C)

This 218 km profile begins at the end of (A–B) profile and shows a close match between the estimated and observed anomalies, with a root mean square error of 2.472 nT (Fig. 11b). It consists of two sections; the upper one represents the sedimentary rocks with a magnetic susceptibility of 0 in c.g.s units and the lower one represents the basements rocks with a magnetic susceptibility of 0.02 in c.g.s. The basement surface depth decreases towards the southwest, with depths ranging from 1000 to 400 meters below the surface.

2D profile (D–E)

This profile overlaps with the end of the B–C profile and has a total length of approximately 282 km. It shows a close match between the estimated and observed anomalies, with a root mean square error 2.446 nT (Fig. 11c). It consists of two main parts: the sedimentary rocks (yellow), which are assigned a magnetic susceptibility of 0 in c.g.s. units, indicating a lack

of magnetization, and the basement rocks (red), located beneath the sedimentary cover. The basement rocks are more magnetized, with a magnetic susceptibility of 0.02 in c.g.s. Along the profile, these basement rocks are relatively deep in the northeast but become shallower toward the southwest.

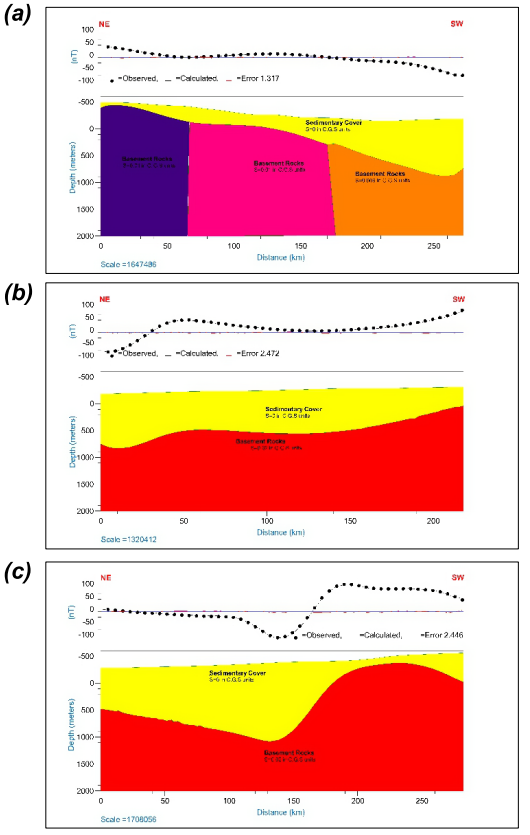

Fig. 11. (a) Two-dimensional magnetic modelling along profile A–B, (b) Two-dimensional magnetic modelling along profile B–C, (c) Two-dimensional magnetic modelling along profile D–E.

The quantitative magnetic modelling carried out helped greatly in delineating depth to the basement and basin framework of the area. We can conclude that:

- The models are partitioned into two layers that are, top sedimentary series and basal basement rocks.

- The basement rocks in the models vary in their composition as reflected by wide range of magnetic susceptibility of different blocks.
- All valleys in the study area, along the modeled profile are associated with subsided basement blocks with different throws.
- The modelled section along these profiles indicates that the depth to the basement surface reaches to 400 m at the northeastern part (near Toshka project).

3.2.4. The subsurface structural framework map

To accomplish this work, space geophysical data was used, such as: GRACE gravity, magnetic, SRTM and geoid. The use of qualitative and quantitative interpretation was considered to throw more light on the subsurface geological picture and structure framework. The well integration of this data with geology gives helpful information. The examination of the interpreted regional structure map (Fig. 12) can lead to see that, the surface of the basement rocks is highly rugged and mostly controlled by structures

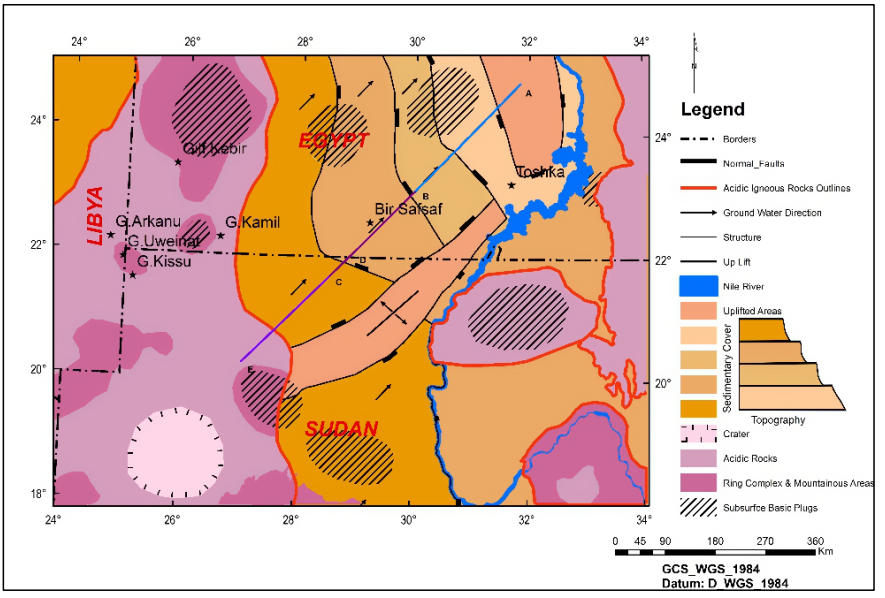

Fig. 12. Interpreted subsurface structural basement map of the study area.

which have a direct effect on thickness variation of the sedimentary cover all over the area.

The predominant structures affecting the sedimentary cover were traced and analysed:

- A series of parallel faults that, all inclined in the same directions (normal faults), gives rise to step faults. Each step is a fault block, and its top may be horizontal or tilted.
- Regionally, the area is characterized by two major intracratonic basins (the Dakhla Basin and the Nile valley Basin) separated by the Kharga uplift and bounded at the south by a NE–SW trending swell of the Uweinat-Bir Safsaf-Aswan uplift.
- The thickness of the sedimentary cover is changed laterally from south to north and from west to east. Changes may be structurally or lithologically controlled, forming the main water aquifer in the study area. This observation is in line with the findings of *Hamdan and Sawires (2013); Nabawy et al. (2019); Robinson et al. (2007)* who demonstrated that the Nubian Aquifer in Egypt primarily extends in a northeast-southwest direction. Therefore, these localities are characterized by the presence of big amount of ground water.
- Magnetic and gravity anomalies allowed us to map the distribution of various basement rock units that have acidic composition with some basic intrusions penetrate the boundary faults and fractures.
- The southwestern Desert of Egypt, the eastern side of Libya, the northwestern Sudan shows the presence of circular depressions in the surface with possible volcanic activity (large field of volcanic craters), the region surrounding the Gilf Kebir plateau, and the top of the plateau itself, are covered by unusual several crater-like forms.

4. Conclusions

This study provides valuable insights into the geological evolution and structural framework of the East Uweinat Ring Complexes Province and the basement structural framework of the Saharan continental crust in Egypt. The integration of EMAG, GRACE, geoid, and SRTM data allowed for a comprehensive interpretation of the subsurface geology.

Through the application of various analytical techniques, this study has uncovered significant structural patterns. The most important conclusions can be outlined as follows.

1. Basement depth and structural trends:
   - Depth estimation using Peter's half-slope method identified significant basement depth variations, ranging from 130 m to 680 m across the study area.
   - The 2D magnetic modelling results confirmed that the basement surface is highly undulating, with clear NE–SW structural trends, consistent with regional tectonic features.
   - The rugged surface of the basement rocks is primarily controlled by structures, influencing the thickness variation of the sedimentary cover throughout the area.
2. Geophysical interpretation of basement structures:
   - The magnetic and gravity maps reveal dominant NE–SW, WNW–ESE, NNW–SSE, and E–W trends associated with both near-surface and deep structures in the study area.
   - Magnetic and gravity anomalies allowed for mapping the distribution of various basement rock units with acidic composition, along with some basic intrusions that penetrate boundary faults and fractures.
   - The subsurface structural framework reveals two major intracratonic basins (Dakhla and Nile Valley Basins), separated by the Kharga uplift and bounded by the Uweinat-Bir Safsaf-Aswan uplift to the south.
   - The southwestern part of the Western Desert of Egypt, the eastern side of Libya, and northwestern Sudan exhibit circular depressions on the surface, which may be related to volcanic activity.
   - Magnetic and gravity anomalies indicate the presence of fault-bounded basement blocks, step faults, and possible intrusive bodies, influencing the sedimentary cover thickness.
3. Implications and future work:
   - The results contribute to a better understanding of the basement structural evolution of the Saharan continental crust in Egypt, which

has implications for hydrocarbon and groundwater exploration.

- Future research should integrate higher-resolution aeromagnetic data and alternative depth estimation methods to refine the structural framework further.

This study highlights the complexity of the basement structures in Egypt and their influence on the overlying sedimentary basins. While the current approach provides valuable insights, additional high-resolution geophysical data and field validation will further enhance our understanding of the region's tectonic evolution.

References

Abdelsalam M. G., Gao S. S., Liégeois J.-P., 2011: Upper mantle structure of the Saharan Metacraton. J. Afr. Earth Sci., **60**, 5, 328–336, doi: 10.1016/j.jafrearsci.2011.03.009.

Abdelsalam M. G., Liégeois J.-P., Stern R. J., 2002: The Saharan Metacraton. J. Afr. Earth Sci., **34**, 3–4, 119–136, doi: 10.1016/S0899-5362(02)00013-1.

Aboelkhair H., Rabei M., 2013: Delineation of the subsurface structures and basement surface of the Abu-Rodaym area, Southwestern Sinai, using ground magnetic data. Earth Planets Space, **65**, 7, 749–757, doi: 10.5047/eps.2012.12.006.

Bakheit A. A., Abdel Aal G. Z., El-Haddad A. E., Ibrahim M. A., 2014: Subsurface tectonic pattern and basement topography as interpreted from aeromagnetic data to the south of El-Dakhla Oasis, western desert, Egypt. Arab. J. Geosci., **7**, 6, 2165–2178, doi: 10.1007/S12517-013-0896-3.

Bea F., Montero P., Abu Anbar M., Molina J. F., Scarrow J. H., 2011a: The Bir Safsaf Precambrian inlier of South West Egypt revisited. A model for $\sim$1.5Ga T_{DM} late Pan-African granite generation by crustal reworking. Lithos, **125**, 3–4, 897–914, doi: 10.1016/j.lithos.2011.05.004.

Bea F., Montero P., Abu Anbar M., & Talavera C., 2011b: SHRIMP dating and Nd isotope geology of the Archean terranes of the Uweinat-Kamil inlier, Egypt–Sudan–Libya. Precambrian Res., **189**, 3–4, 328–346, doi: 10.1016/j.precamres.2011.07.017.

Benahmed Daho S. A., Mendas A., Fairhead J. D., Derkaoui A., 2009: Impact of the new GRACE Geopotential Model and SRTM data on the geoid modelling in Algeria. J. Geodyn., **47**, 2–3, 63–71, doi: 10.1016/J.JOG.2008.07.006.

Bernau R., Darbyshire D. P. F., Franz G., Harms U., Huth A., Mansour N., Pasteels P., Schandelmeier H., 1987: Petrology, geochemistry and structural development of the Bir Safsaf-Aswan uplift, Southern Egypt. J. Afr. Earth Sci., **6**, 1, 79–90, doi: 10.1016/0899-5362(87)90109-6.

Blades M. L., Collins A. S., Foden J., Payne J. L., Stüwe K., Abu-Alam T., Makroum F., Hassan M., 2021: Age and hafnium isotope evolution of Sudanese Butana and

Chad illuminates the Stenian to Ediacaran evolution of the south and east Sahara. Precambrian Res., **362**, 106323, doi: 10.1016/j.precamres.2021.106323.

Braun A., 2021: Retrieval of digital elevation models from Sentinel-1 radar data – open applications, techniques, and limitations. Open Geosci., **13**, 1, 532–569, doi: 10.1515/geo-2020-0246.

Butler D. K., 2007: Engineering and environmental applications of the potential field methods of geophysics. Proc. Symposium on the Application of Geophysics to Engineering and Environmental Problems 2007, 310–322, doi: 10.4133/1.2924683.

Chen J., Cazenave A., Dahle C., Llovel W., Panet I., Pfeffer J., Moreira L., 2022: Applications and Challenges of GRACE and GRACE Follow-On Satellite Gravimetry. Surv. Geophys., **43**, 1, doi: 10.1007/s10712-021-09685-x.

Choubert G., Faure-Muret A., 1990: International geological map of Africa (third edition, scale 1:5,000,000). Commission for the Geological Map of the World, Paris, France.

Corchete V., 2010: The high-resolution gravimetric geoid of Italy: ITG2009. J. Afr. Earth Sci., **58**, 3, 580–584, doi: 10.1016/j.jafrearsci.2010.05.010.

El-Gaby S., List, F. K., Tehrani R., 1988: Geology, evolution and metallogenesis of the Pan-African Belt in Egypt. In: El-Gaby S., Greiling R. O. (Eds.): The Pan-African Belt of northeast Africa and adjacent areas: Tectonic evolution and economic aspects of a Late Proterozoic Orogen, Vieweg and Sohn, pp. 17–68, Braunschweig, Wiesbaden.

Fairhead J. D., Okereke C. S., 1988: Depths to major density contrasts beneath the West African rift system in Nigeria and Cameroon based on the spectral analysis of gravity data. J. Afr. Earth Sci. (and the Middle East), **7**, 5–6, 769–777, doi: 10.1016/0899-5362(88)90018-8.

Fezaa N., Liégeois J.-P., Abdallah N., Cherfouh E. H., De Waele B., Bruguier O., Ouabadi A., 2010: Late Ediacaran geological evolution (575–555 Ma) of the Djanet Terrane, Eastern Hoggar, Algeria, evidence for a Murzukian intracontinental episode. Precambrian Res., **180**, 3–4, 299–327, doi: 10.1016/j.precamres.2010.05.011.

Fritz H., Abdelsalam M., Ali K. A., Bingen B., Collins A. S., Fowler A. R., Ghebreab W., Hauzenberger C. A., Johnson P. R., Kusky T. M., Macey P., Muhongo S., Stern R. J., Viola G., 2013: Orogen styles in the East African Orogen: A review of the Neoproterozoic to Cambrian tectonic evolution. J. Afr. Earth Sci., **86**, 65–106, doi: 10.1016/j.jafrearsci.2013.06.004.

Geosoft Oasis montaj – Seequent (n.d.): Data processing and analysis systems for Earth science applications. Geosoft Inc., Toronto, accessed November 21, 2023 from https://www.seequent.com/products-solutions/geosoft-oasis-montaj/.

Giresse P., 2008: Tropical and sub-tropical West Africa: marine and continental changes during the late Quaternary. Developments in Quaternary Sciences series, vol. 10, Elsevier, Amsterdam, The Netherlands, 395 p.

Gubanov A. P., Mooney W. D., 2009: New global geological maps of crustal basement age. AGU Fall Meeting 2009 abstracts, T53B-1583, https://ui.adsabs.harvard.edu/abs/2009AGUFM.T53B1583G/abstract.

Haas P., Ebbing J., Celli N. L., Rey P. F., 2021: Two-step gravity inversion reveals variable architecture of African Cratons. Front. Earth Sci., **9**, 696674, doi: 10.3389/feart.2021.696674.

Hamdan A. M., Sawires R. F., 2013: Hydrogeological studies on the Nubian sandstone aquifer in El-Bahariya Oasis, Western Desert, Egypt. Arab. J. Geosci., **6**, 5, 1333–1347, doi: 10.1007/S12517-011-0439-8.

Hanafy S. M. M., 2014: The late Precambrian/Cambrian hot spot activity and their implications for hydrocarbon resources in Egypt. J. Egypt. Geophys. Soc., **12**, 1, 79–87, doi: 10.21608/jegs.2014.385014.

Harris N. B. W., Hawkesworth C. J., Ries A. C., 1984: Crustal evolution in north-east and east Africa from model Nd ages. Nature, **309**, 5971, 773–776, doi: 10.1038/309773a0.

Hesse K.-H., Hissene A., Kheir O., Schnäcker E., Schneider M., Thorweihe U., 1987: Hydrogeological investigations in the Nubian aquifer system, eastern Sahara. In: Kilitzsch E., Schranck E. (Eds.): Research in Egypt and Sudan, Dietrich Reimer, Berliner Geowiss. Abh. (A), **75**, 2, Berlin, 379–464.

Hinze W. J., von Frese R. R. B., Saad A. H., 2013: The gravity method. In: Hinze W. J., von Frese R. R. B., Saad A. H. (Eds.): Gravity and Magnetic Exploration. Cambridge University Press, 19–37, doi: 10.1017/CBO9780511843129.003.

Ibrahim A., Gemail K. S., Bedair S., Saada S. A., Koch M., Nosair A., 2023: An integrated approach to unravel the structural controls on groundwater potentialities in hyper-arid regions using satellite and land-based geophysics: A case study in Southwestern Desert of Egypt. Surv. Geophys., **44**, 3, 783–819, doi: 10.1007/s10712-022-09755-8.

ICGEM (n.d.): International Centre for Global Gravity Field Models. GFZ Potsdam, accessed June 25, 2024 from https://icgem.gfz-potsdam.de/home.

Issawi B., 1980: Geology, stratigraphy and structure of Southwest Egypt. Geogr. J., **146**, 1, 72–75, doi: 10.2307/634073.

Jessell M. W., Begg G. C., Miller M. S., 2016: The geophysical signatures of the West African Craton. Precambrian Res., **274**, 3–24, doi: 10.1016/j.precamres.2015.08.010.

Jux U., Issawi B., 1983: Cratonic sedimentation in Egypt during the Paleozoic. Ann. Geol. Surv. Egypt, **13**, 223–245.

Karmakar S., Schenk V., 2015: Neoarchean UHT metamorphism and paleoproterozoic UHT reworking at Uweinat in the East Sahara Ghost Craton, SW Egypt: Evidence from petrology and texturally controlled in situ monazite dating. J. Petrol., **56**, 9, 1703–1742, doi: 10.1093/petrology/egv051.

Kearey P., Brooks M., 1991: An introduction to geophysical exploration. 2nd ed. Blackwell Scientific Publications, Oxford, 254 p.

Kennedy W. Q., 1964: The structural differentiation of Africa in the Pan-African (500 m.y.) tectonic episode. Res. Inst. African Geol., Univ. Leeds, 8th Ann. Rept., 8, 48–49.

Keppie J. D., Dostal J., Murphy J. B., 2011: Complex geometry of the Cenozoic magma plumbing system in the central Sahara, NW Africa. Int. Geol. Rev., **53**, 14, 1576–1592, doi: 10.1080/00206814.2010.496211.

Khalil A., Abdel Hafeez T. H., Saleh H. S., Mohamed W. H., 2016: Inferring the subsurface basement depth and the structural trends as deduced from aeromagnetic data at West Beni Suef area, Western Desert, Egypt. NRIAG J. Astron. Geophys., **5**, 2, 380–392, doi: 10.1016/j.nrjag.2016.08.001.

Klitzsch E., Lejal-Nicol A., 1984: Flora and fauna from a strata in southern Egypt and northern Sudan (Nubia and surrounding areas). Berl. Geowiss. Abh. **50**, A, 47–79.

Küster D., Liégeois J.-P., Matukov D., Sergeev S., Lucassen F., 2008: Zircon geochronology and Sr, Nd, Pb isotope geochemistry of granitoids from Bayuda Desert and Sabaloka (Sudan): Evidence for a Bayudian event (920–900 Ma) preceding the Pan-African orogenic cycle (860–590 Ma) at the eastern boundary of the Saharan Metacraton. Precambrian Res., **164**, 1–2, 16–39, doi: 10.1016/j.precamres.2008.03.003.

Le Pape F., Jones A. G., Jessell M. W., Hogg C., Siebenaller L., Perrouty S., Touré A., Ouiya P., Boren G., 2021: The nature of the southern West African craton lithosphere inferred from its electrical resistivity. Precambrian Res., **358**, 106190, doi: 10.1016/j.precamres.2021.106190.

Lebedev S., Boonen J., Trampert J., 2009: Seismic structure of Precambrian lithosphere: New constraints from broad-band surface-wave dispersion. Lithos, **109**, 1–2, 96–111, doi: 10.1016/j.lithos.2008.06.010.

Lemenkova P., 2023: Seafloor and Ocean Crust Structure of the Kerguelen Plateau from Marine Geophysical and Satellite Altimetry Datasets. Geomatics, **3**, 3, 393–426, doi: 10.3390/geomatics3030022.

Liégeois J.-P., Abdelsalam M. G., Ennih N., Ouabadi A., 2013: Metacraton: Nature, genesis and behavior. Gondwana Research, **23**, 1, 220–237, doi: 10.1016/J.GR.2012.02.016.

Liu S., Hu X., 2018: Inversion and Interpretation of Magnetic Anomaly in the Presence of Significant Remanence and Self-Demagnetization Based on Magnetic Amplitude. In: Okiwelu A. (Ed.): Geophysics. IntechOpen, doi: 10.5772/intechopen.71027.

Maune D. F., Kopp S. M., Crawford C. A., Zervas C. E., 2007: Introduction. In: Maune D. F. (Ed.): Digital Elevation Model Techniques and Applications: The DEM Users Manual, 2nd ed., pp. 1–35, Am. Soc. for Photogramm. and Remote Sens., Bethesda, Md.

Maus S., 2009: EMAG2: Earth Magnetic Anomaly Grid (2-arc-minute resolution), ver. 2. NOAA National Centers for Environmental Information. doi: 10.7289/V5MW2F2P, accessed June 25, 2024, from https://www.ncei.noaa.gov/products/earth-magnetic-model-anomaly-grid-2.

Mehanee S. A., 2022: Simultaneous Joint Inversion of Gravity and Self-Potential Data Measured along Profile: Theory, Numerical Examples, and a Case Study from Mineral Exploration with Cross Validation from Electromagnetic Data. IEEE Trans. Geosci. Remote Sens., **60**, 4701620, doi: 10.1109/TGRS.2021.3071973.

Mohamed A., Ahmed E., Alshehri F., Abdelrady A., 2022: The Groundwater Flow Behavior and the Recharge in the Nubian Sandstone Aquifer System during the Wet and Arid Periods. Sustainability, **14**, 11, 6823, doi: 10.3390/SU14116823.

Mohamed A., Sultan M., Ahmed M., Yan E., Ahmed E., 2017: Aquifer recharge, depletion, and connectivity: Inferences from GRACE, land surface models, and geochemical and geophysical data. Geol. Soc. Am. Bull., 129, 5–6, 534–546, doi: 10.1130/B31460.1.

Mono J. A., Bouba A., Nguiya S., 2024: Edge detection and depth estimation using a tilt angle and Euler deconvolution from combined terrestrial and GRACE gravity data of the Adamawa Plateau Region (North-Cameroon). IOSR J. Appl. Phys. (IOSR-JAP), **16**, 4, Ser. 1, 11–19, doi: 10.9790/4861-1604011119.

Nabawy B. S., Abdelhalim A., El-Meselhy A., 2019: Step-drawdown test as a tool for the assessment of the Nubia sandstone aquifer in East El-Oweinat Area, Egypt. Environ. Earth Sci., **78**, 13, 375, doi: 10.1007/S12665-019-8375-0.

Nour S., 1996: Groundwater potential for irrigation in the East Oweinat area, Western Desert, Egypt. Environ. Geol., **27**, 3, 143–154, doi: 10.1007/bf00770426.

Olugboji T., Xue S., Legre J.-J., Tamama Y., 2024: Africa's crustal architecture inferred from probabilistic and perturbational inversion of ambient noise: ADAMA. Geochem. Geophys. Geosyst., **25**, 1, e2023GC011086, doi: 10.1029/2023GC011086.

Pavlis N. K., Holmes S. A., Kenyon S. C., Factor J. K., 2012: The development and evaluation of the Earth Gravitational Model 2008 (EGM2008). J. Geophys. Res. Solid Earth, **117**, B4, B04406, doi: 10.1029/2011JB008916.

Persits F. M., Ahlbrandt T. S., Tuttle M. L., Charpentier R. R., Brownfield M. E., Takahashi K. I., 1997: Map showing geology, oil and gas fields, and geologic provinces of Africa. U.S. Geological Survey, doi: 10.3133/ofr97470A.

Peters L. J., 1949: The direct approach to magnetic interpretation and its practical application. Geophysics, **14**, 3, 290–320, doi: 10.1190/1.1437537.

Prasad K. N. D., Singh A. P., Rao P. R., Prakash O., Begum S. K., 2021: Multistage magmatic intrusion in Narmada–Tapti region, India: Insights from geopotential modelling. J. Earth Syst. Sci., **130**, 4, 227, doi: 10.1007/s12040-021-01721-z.

Richter A., 1986: Geologie der metamorphen und magmatischen Gesteine im Gebiet zwischen Gebel Uweinat und Gebel Kamil–SW Aegypten/NW Sudan (Geology of the metamorphic and igneous rocks in the area between Gebel Uweinat and Gebel Kamil–SW Egypt/NW Sudan). Berliner Geowiss. Abh., **73**, A, 201 p. (in German with English summary).

Robinson C. A., Werwer A., El-Baz F., El-Shazly M., Fritch T., Kusky T., 2007: The Nubian Aquifer in Southwest Egypt. Hydrogeol. J., **15**, 1, 33–45, doi: 10.1007/S10040-006-0091-7.

Saad M. H., El-Khadragy A. A., Shabaan M. M., Azab A., 2010: An integrated study of gravity and magnetic data on South Sitra area, Western Desert, Egypt. J. Appl. Sci. Res., **6**, 6, 616–636.

Schandelmeier H., Richter A., Franz G., 1983: Outline of the geology of magmatic and metamorphic units between Gebel Uweinat and Bir Safsaf (SW Egypt/NW Sudan). J. Afr. Earth Sci., **1**, 3–4, 275–283, doi: 10.1016/s0731-7247(83)80012-3.

Schillaci C., Braun A., Kropáček J., 2015: Terrain analysis and landform recognition. In: Clarke L., Nield J. (Eds.): Geomorphological Techniques, British Society for Geomorphology, London.

Senosy M. M., Youssef M. M., Abdel Zaher M., 2013: Sedimentary cover in the South Western Desert of Egypt as deduced from Bouguer gravity and drill-hole data. J. Afr. Earth Sci., **82**, 1–14, doi: 10.1016/j.jafrearsci.2013.02.001.

Shellnutt J. G., Yeh M.-W., Lee T.-Y., Iizuka Y., Pham N. H. T., Yang C.-C., 2018: The origin of Late Ediacaran post-collisional granites near the Chad Lineament, Saharan Metacraton, South-Central Chad. Lithos, **304–307**, 450–467, doi: 10.1016/j.lithos.2018.02.020.

Shellnutt J. G., Yeh M.-W., Pham N. H. T., Lee T.-Y., 2019: Cryptic regional magmatism in the southern Saharan Metacraton at 580 Ma. Precambrian Res., **332**, 105398, doi: 10.1016/j.precamres.2019.105398.

Sobh M., Ebbing J., Mansi A. H., Götze H.-J., Emry E. L., Abdelsalam M. G., 2020: The Lithospheric Structure of the Saharan Metacraton From 3-D Integrated Geophysical-Petrological Modeling. J. Geophys. Res. Solid Earth, **125**, 8, e2019JB018747, doi: 10.1029/2019JB018747.

Steinberger B., 2016: Topography caused by mantle density variations: observation-based estimates and models derived from tomography and lithosphere thickness. Geophys. J. Int., **205**, 1, 604–621, doi: 10.1093/gji/ggw040.

Steinberger B., Rathnayake S., Kendall E., 2021: The Indian Ocean Geoid Low at a plume-slab overpass. Tectonophysics, **817**, 229037, doi: 10.1016/j.tecto.2021.229037.

Stern R. J., 2018: Neoproterozoic formation and evolution of Eastern Desert continental crust – The importance of the infrastructure-superstructure transition. J. Afr. Earth Sci., **146**, 15–27, doi: 10.1016/j.jafrearsci.2017.01.001.

Sudan Environment Report, 2020: Sudan First State of Environment and Outlook Report 2020, UNEP – UN Environment Programme. (n.d.). Retrieved August 9, 2024, from https://www.unep.org/resources/report/sudan-first-state-environment-outlook-report-2020.

Sun Y., Zeng X., Yang W., Li X., Zhang W., Zhang X., 2023: Mapping structural lineaments using the edge filters of the potential field: a case study of the Rizhao–Lianyungang area, East China. Front. Earth Sci., **11**, doi: 10.3389/feart.2023.1162187.

Talwani M., Worzel J. L., Landisman M., 1959: Rapid gravity computations for two-dimensional bodies with application to the Mendocino submarine fracture zone. J. Geophys. Res., **64**, 1, 49–59, doi: 10.1029/JZ064I001P00049.

Tapley B., Ries J., Bettadpur S., Chambers D., Cheng M., Condi F., Gunter B., Kang Z., Nagel P., Pastor R., Pekker T., Poole S., Wang F., 2005: GGM02 – An improved Earth gravity field model from GRACE. J. Geod., **79**, 467–478, doi: 10.1007/s00190-005-0480-z.

Thorweihe U., 1986: Isotopic identification and mass balance of the Nubian Aquifer System in Egypt. In: Thorweihe U. (Ed.): Impact of climatic variations on East Sahar-

ian Groundwaters, Modeling of large scale flow regimes, Proceedings of "Workshop on hydrology", Berliner Geowiss. Abh., (A), **72**, 55–78.

U.S. Geological Survey, 2019: EarthExplorer-Home. Satellite Data. Accessed June 25, 2024, from https://earthexplorer.usgs.gov/.

Vail J., 1976: Location and geochronology of igneous ring-complexes and related rocks in north-east Africa. Geol. Jahrb., B20, 97–114.

Van Hinsbergen D. J. J., Buiter S. J. H., Torsvik T. H., Gaina C., Webb S. J., 2011: The formation and evolution of Africa from the Archaean to present: Introduction. Geol. Soc. Spec. Publ., **357**, 1, 1–8, doi: 10.1144/SP357.1.

Won I. J., Bevis M., 1987: Computing the gravitational and magnetic anomalies due to a polygon; algorithms and Fortran subroutines. Geophysics, **52**, 2, 232–238, doi: 10.1190/1.1442298.

Wu X., Xing J., Li C., Liu X., Yang K., Chen H., Gong W., 2018: Application of Geoid Anomalies to the Tectonic Research in the East Asian Continental Margin. J. Ocean Univ. China, **17**, 811–822, doi: 10.1007/s11802-018-3589-4.

Zimmer M., Kröner A., Jochum K. P., Reischmann T., Todt W., 1995: The Gabal Gerf complex: A precambrian N-MORB ophiolite in the Nubian Shield, NE Africa. Chem. Geol., **123**, 1–4, 29–51, doi: 10.1016/0009-2541(95)00018-H.